THE JOURNAL OF PHYSICAL CHEMISTRY C

Article

pubs.acs.org/JPCC

Effect of the Partial Replacement of CaH_2 with CaF_2 in the Mixed System $CaH_2 + MgB_2$

C. Pistidda,*[,†] F. Karimi,[†] S. Garroni,[‡] A. Rzeszutek,[†] C. Bonatto Minella,[†,◇] C. Milanese,[§] T. T. Le,[†] L. H. Rude,[∥] J. Skibsted,[∥] T. R. Jensen,[∥] C. Horstmann,[†] C. Gundlach,[⊥] M. Tolkiehn,[#] P. K. Pranzas,[†] A. Schreyer,[†] T. Klassen,[†] and M. Dornheim[†]

[†]Institute of Materials Research, Materials Technology, Helmholtz-Zentrum Geesthacht, Max-Planck-Strasse 1, D-21502 Geesthacht, Germany

[‡]Dipartimento di Chimica, Università di Sassari and INSTM, Via Vienna 2, I-07100 Sassari, Italy

[§]Pavia H2 Lab, C.S.G.I. & Dipartimento di Chimica, Sezione di Chimica Fisica, Università di Pavia, Viale Taramelli 16, I-27100 Pavia, Italy

[∥]Center for Materials Crystallography, iNANO, and Department of Chemistry, Aarhus University, Langelandsgade 140, DK-8000 Aarhus, Denmark

[⊥]MAX-lab, S-22100 Lund, Sweden

[#]DESY Synchrotron, Beamline D3, Hamburg, Germany

ABSTRACT: In this work the effect of a partial replacement of CaH_2 with CaF_2 on the sorption properties of the system $CaH_2 + MgB_2$ has been studied. The first five hydrogen absorption and four desorption reactions of the $CaH_2 + MgB_2$ and $3CaH_2 + CaF_2 + 4MgB_2$ systems were investigated by means of volumetric measurements, high-pressure differential scanning calorimetric technique (HP-DSC), ^{11}B and ^{19}F MAS NMR spectroscopy, and in situ synchrotron radiation powder X-ray diffraction (SR-PXD). It was observed that already during the mixing of the reactants formation of a nonstoichiometric $CaF_{2-x}H_x$ solid solution takes place. Formation of the $CaF_{2-x}H_x$ solid solution sensibly affects the overall hydrogen sorption reactions of the system $CaH_2 + MgB_2$.

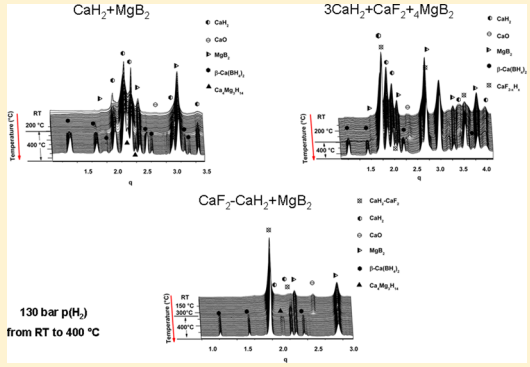

INTRODUCTION

In the past years borohydrides and hydride mixtures of borohydrides have been extensively studied as possible candidates for hydrogen storage.[1−25] Due to its high gravimetric and volumetric hydrogen capacity, $Ca(BH_4)_2$ represents an ideal candidate for storing hydrogen. The calculated enthalpy value for the decomposition reaction of the pristine calcium borohydrides lies between 31.09 and 68.51 kJ mol^{-1} H_2.[22,23,26−28] This uncertainty in the decomposition enthalpy value is due to the presence of five possible decomposition reaction mechanisms. The decomposition reaction mechanisms proposed in the literature for $Ca(BH_4)_2$ are as follows

$$Ca(BH_4)_2 \leftrightarrow 2/3CaH_2 + 1/3CaB_6 + 10/3H_2 \quad (37.04\,kJ\,mol^{-1}H_2) \tag{1}$$

from ref 28

$$Ca(BH_4)_2 \leftrightarrow CaH_2 + 2B + 3H_2 \quad (57.3\,kJ\,mol^{-1}H_2) \tag{2}$$

from ref 26

$$Ca(BH_4)_2 \leftrightarrow 1/6CaB_{12}H_{12} + 5/6CaH_2 + 13/6H_2 \quad (31.34−39.2\,kJ\,mol^{-1}H_2) \tag{3}$$

from refs 27 and 28

$$Ca(BH_4)_2 \leftrightarrow CaB_2H_6 + H_2 \quad (31.09\,kJ\,mol^{-1}H_2) \tag{4}$$

from ref 28

$$Ca(BH_4)_2 \leftrightarrow CaB_2H_2 + 3H_2 \quad (68.51\,kJ\,mol^{-1}H_2) \tag{5}$$

from ref 28.

The enthalpy values of reactions 1−4 are calculated assuming the reaction takes place at 300 K and 1 bar of H_2 pressure, whereas the enthalpy value given for reaction 5 is calculated at 0 K neglecting the zero-point energy contribution. However, the possibility that decomposition of $Ca(BH_4)_2$ takes place following more than a single reaction path is possible. Recently, Kim et al. reported that the desorption reaction of $Ca(BH_4)_2$,

Received: August 30, 2014
Revised: November 17, 2014
Published: November 17, 2014

   dx.doi.org/10.1021/jp508780b | J. Phys. Chem. C 2014, 118, 28409−28417

performed at 1 bar of hydrogen pressure at a final temperature of 500 °C, leads to formation of CaB_6 and $CaB_{12}H_{12}$ passing through formation of an unidentified amorphous phase and CaB_2H_x.[26]

Although CaB_2H_x and CaB_6 are known to react with CaH_2 to form $Ca(BH_4)_2$, formation of stable products such as $CaB_{12}H_{12}$ and amorphous boron significantly reduces the reversibility of $Ca(BH_4)_2$.[4,29,30] In this regard, a maximum reversibility of about 60% was reported to be possible only after addition of selected halogenated additives (e.g., NbF_5 and $TiCl_4$).[22,31,32] These additives appear to direct the desorption reaction path of $Ca(BH_4)_2$ toward formation of CaB_6 rather than other stable boron compounds. Barkhordarian et al. showed that complete formation of $Ca(BH_4)_2$ and MgH_2 is possible by hydrogenation of the mixture $CaH_2 + MgB_2$.[5] This system has a hydrogen gravimetric capacity of 10.5 wt %, and like for $Ca(BH_4)_2$ several decomposition reaction paths are predicted to be possible[26]

$$Ca(BH_4)_2 + MgH_2 \leftrightarrow CaH_2 + MgB_2 + 4H_2 \quad (46.9\ kJ\ mol^{-1}\ H_2) \tag{6}$$

from ref 26

$$Ca(BH_4)_2 + MgH_2 \leftrightarrow 2/3CaH_2 + 1/3CaB_6 + Mg + 13/3H_2 \quad (45\ kJ\ mol^{-1}\ H_2) \tag{7}$$

from ref 26

$$Ca(BH_4)_2 + MgH_2 \leftrightarrow CaH_2 + 2B + Mg + 3H_2 \quad (57.9\ kJ\ mol^{-1}\ H_2) \tag{8}$$

from ref 26.

Differently from $Ca(BH_4)_2$, the dehydrogenation reaction of the system $Ca(BH_4)_2 + MgH_2$ is partially reversible without the need of any additives.[16] Bonatto Minella et al. recently reported experimental evidence that during the hydrogen desorption of $Ca(BH_4)_2 + MgH_2$ formation of $CaB_{12}H_{12}$ also can take place.[16] The possibility to modify the thermodynamic properties of complex hydrides was recently reported to be possible by replacing one or more hydrogen atoms with fluorine atoms. This experimental approach is called the functional anion concept.[33,34] A material to which this concept successfully applies is $NaAlH_4$.[33] The possibility to modify the thermodynamic properties of $Ca(BH_4)_2$ in the mixed system $Ca(BH_4)_2 + MgH_2$ is highly appealing. This might result in a different decomposition reaction path, allowing formation of products with a higher degree of reversibility (i.e., MgB_2 and/or CaB_6 only).

In this work the effect of a partial replacement of CaH_2 with CaF_2 on the sorption properties of the system $CaH_2 + MgB_2$ was investigated, and the results were compared with those obtained for the pristine system $CaH_2 + MgB_2$. In order to perform this study, ex situ powder X-ray diffraction (PXD), in situ synchrotron radiation powder X-ray diffraction (SR-PXD), high-pressure titration (volumetric measurement), high-pressure differential scanning calorimetric technique (HP-DSC), and solid state magic angle spinning nuclear magnetic resonance spectroscopy (MAS NMR) were applied.

EXPERIMENTAL DETAILS

CaH_2 (98% purity) and MgB_2 (98% purity) were purchased from Alfa Aesar; CaF_2 (99.99% purity) was purchased from Sigma-Aldrich. As a reference, a solid solution of CaF_2−CaH_2 in a molar ratio of 1:1 was prepared by ball milling for 5 h using a hardened steel vial, a ball to powder ratio of 30:1, and a Fritsch P5 planetary mill at a rotational regime of 230 rpm. The milled material was then heated up to 400 °C under an inert atmosphere and kept at 400 °C for 24 h. In the article, this reference mixture will be mentioned as CaF_2−CaH_2 solid solution, whereas the general solid solution of CaF_2 and CaH_2 will be addressed as $CaF_{2-x}H_x$. The systems $CaH_2 + MgB_2$, $3CaH_2 + CaF_2 + 4MgB_2$, and $CaF_2 - CaH_2 + MgB_2$ were prepared charging the compounds into alumina vials and milling them for 10 h using a planetary mill with a ball to powder ratio of 30:1 and a rotational regime of 230 rpm. Handling and milling were performed in a dedicated glovebox under a continuously purified argon atmosphere. The hydrogen absorption and desorption of the material were performed in a PCTPro-2000 volumetric apparatus (SETARAM Instruments). The as-milled material and material after hydrogen desorption were hydrogenated at a temperature of 380 °C and hydrogen pressure of 130 bar for 20 h.

Unfortunately, due to instrumental limitations, the hydrogen absorption curves could not be recorded, and for this reason they will not be shown in this work.

Desorption measurements were performed under static vacuum conditions (starting pressure of 10^{-2} bar), heating the material from RT to 380 °C with a heating rate of 20 °C/min and keeping it under isothermal conditions at 380 °C for several hours.

Ex situ powder X-ray diffraction analysis was carried out with a Siemens D5000 X-ray diffractometer using Cu Kα radiation. The powder was spread onto a single silicon crystal and sealed in the glovebox with an airtight hood.

In situ SR-PXD measurements were performed at MAX II Synchrotron, at the beamline I711 in the research laboratory MAX-lab, Lund, Sweden, and at DESY synchrotron, at the beamline D3, Hamburg, Germany. The wavelengths used were 0.1100 and 0.0498 nm, respectively. A special sample holder, designed for in situ monitoring of solid/gas reactions, was utilized.[35−37] All raw SR diffraction data were elaborated and converted to powder patterns by use of the FIT2D program.[38] For the sake of comparability of measurements acquired with different wavelengths, diffraction intensities were plotted as a function of scattering vector q, where $q = (4\pi/\lambda)\sin\theta$, λ is the wavelength, and θ is one-half the scattering angle.

^{11}B MAS NMR spectra were obtained on a Varian INOVA-400 (9.39 T) spectrometer using a home-built CP/MAS probe for 5 mm o.d. rotors and a spinning speed of ν_R = 10.0 kHz. Spectra were acquired using the single-pulse experiment with ^1H decoupling during acquisition ($\gamma B_2/2\pi$ = 50 kHz) using a 0.5 μs excitation pulse for the rf field strength, $\gamma B_1/2\pi$ = 55 kHz (10° flip angle), and a relaxation delay 4 s. ^{19}F MAS NMR spectra were acquired at 7.05 T on a Varian INOVA-300 spectrometer, employing a home-built CP/MAS probe for 5 mm o.d. rotors and a spinning speed of ν_R = 10.0 kHz. Single-pulse spectra were obtained without ^1H decoupling, employing a 2.5 μs excitation pulse for $\gamma B_1/2\pi$ = 60 kHz (54° flip angle) and a relaxation delay of 120 s. For all experiments the samples were packed into airtight end-capped zirconia (PSZ) rotors in an argon-filled glovebox. ^{11}B and ^{19}F chemical shifts were referenced to external samples of neat $BF_3{\cdot}O(CH_2CH_3)_2$ and neat CCl_3F, respectively.

Hydrogen absorption reactions were investigated also by high-pressure differential scanning calorimetry (HP-DSC) using a high-pressure calorimeter (Sensys DSC, Setaram).

dx.doi.org/10.1021/jp508780b | J. Phys. Chem. C 2014, 118, 28409−28417

HP-DSC measurements were carried out at a constant pressure of 130 bar of hydrogen from room temperature (RT) to 400 °C, applying a heating rate of 5 °C/min. Handling of the material was always performed in a dedicated glovebox under a continuously purified argon atmosphere.

RESULTS

Hydrogen desorption kinetics measured for hydrogenated $CaH_2 + MgB_2$ and $3CaH_2 + CaF_2 + 4MgB_2$ are presented in Figure 1A and 1B, respectively. The first desorption measurement performed on the hydrogenated $CaH_2 + MgB_2$ was stopped after 6 h, when an amount of hydrogen equal to 6.2 wt % was released. The following desorption measurements were carried out for periods of time longer than 20 h. The hydrogen desorption capacities achieved for further desorption measurements were 5.8, 4.2, and 3.6 wt % for the second, third, and fourth cycle, respectively. The first desorption measurement performed on the hydrogenated $3CaH_2 + CaF_2 + 4MgB_2$ was stopped after 22 h when an amount of hydrogen equal to 4.3 wt % was released. The hydrogen capacities achieved for further desorption measurements were 3.9 wt % after 20 h for the second desorption and 3.3 wt % after approximately 7 h for the third and fourth desorption measurements. The hydrogen desorption reactions of $CaH_2 + MgB_2$ and $3CaH_2 + CaF_2 + 4MgB_2$ appear to take place in a single step.

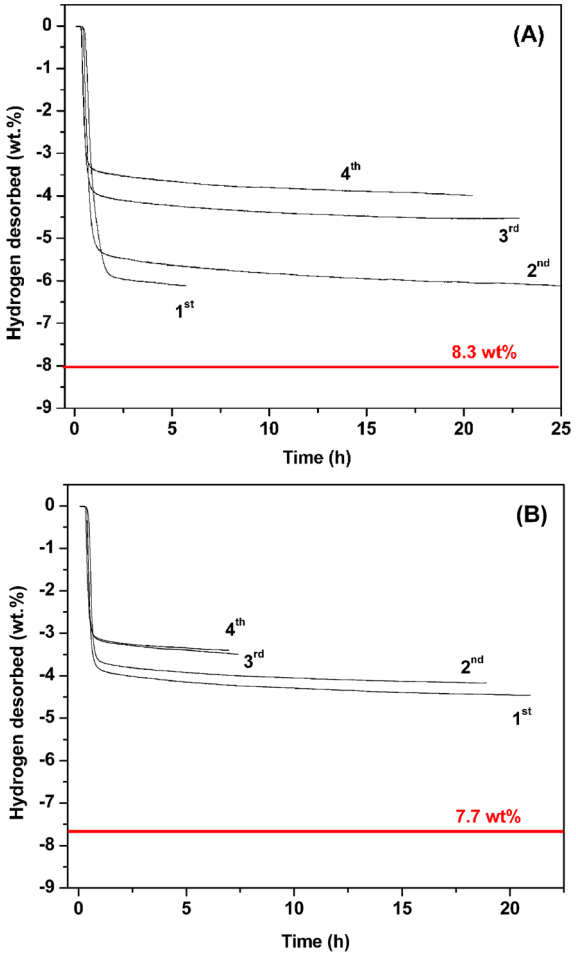

Figure 1. Desorption kinetics of hydrogenated $CaH_2 + MgB_2$ (A) and $3CaH_2 + CaF_2 + 4MgB_2$ (B) measured in a Sievert's-type apparatus. Samples were heated under static vacuum conditions (starting pressure of 10^{-2} bar) from RT to 380 °C, applying a heating rate of 20 °C/min and keeping the material under isothermal conditions at 380 °C for several hours.

In order to understand the reasons for not achieving the theoretical hydrogen capacities, PXD characterization of the starting reactants and absorption products upon cycling was performed. In Figure 2 the PXD patterns of the as-milled $CaH_2 + MgB_2$ (pattern a) and $3CaH_2 + CaF_2 + 4MgB_2$ (pattern a1) and their reaction products after the first (pattern b and b1) and fifth absorption cycle (pattern c and c1) are reported. For both systems, mechanochemical treatment does not lead to formation of new crystalline compounds. Indeed, the Bragg reflections present in the PXD pattern of the ball-milled $CaH_2 + MgB_2$ can be attributed only to CaH_2, MgB_2, and a small amount of CaO, and for the milled $3CaH_2 + CaF_2 + MgB_2$ the observed Bragg reflections are those of CaF_2, CaH_2, MgB_2, and a small amount of CaO. The pattern of $CaH_2 + MgH_2$ after the first hydrogen absorption shows the presence of α-$Ca(BH_4)_2$, $Ca_4Mg_3H_{14}$, and a small amount of unreacted MgB_2. The pattern of $3CaH_2 + CaF_2 + 4MgH_2$ after the first hydrogen absorption shows the presence of α-$Ca(BH_4)_2$, $Ca_4Mg_3H_{14}$, as well as small amounts of MgB_2 and $CaF_{2-x}H_x$. The pattern of $CaH_2 + MgH_2$ after the fifth hydrogen absorption shows the presence of a small amount of α-$Ca(BH_4)_2$ and a large amount of $Ca_4Mg_3H_{14}$. The pattern of $3CaH_2 + CaF_2 + 4MgH_2$ after

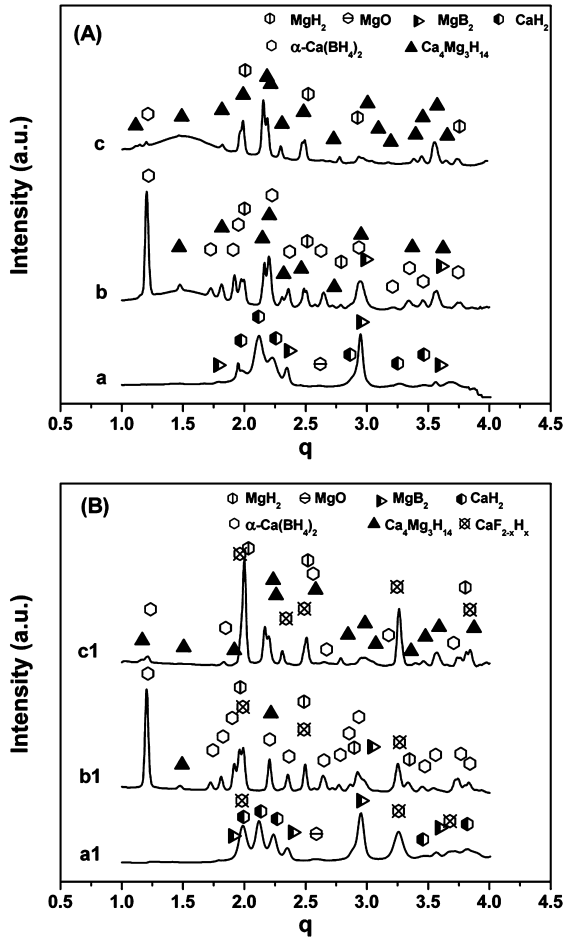

Figure 2. Ex situ PXD characterization of the systems $CaH_2 + MgB_2$ (A) and $3CaH_2 + CaF_2 + 4MgB_2$ (B): as milled (a, a1), after the first hydrogen absorption (b, b1), and after the fifth absorption (c, c1).

dx.doi.org/10.1021/jp508780b | J. Phys. Chem. C 2014, 118, 28409−28417

the fifth hydrogen absorption shows the presence of small amounts of α-$Ca(BH_4)_2$ and $Ca_4Mg_3H_{14}$ but a big amount of $CaF_{2-x}H_x$.

PXD analysis is a powerful tool to gain a wide range of information on crystalline matter. However, due to the possible presence of amorphous compounds, use of solid state MAS NMR techniques is necessary. Thus, the milled CaH_2 + MgB_2 system and its absorption products after the first and fifth absorption cycle were investigated by ^{11}B MAS NMR. The ^{11}B MAS NMR spectrum of the mechanochemically treated CaH_2 + MgB_2 sample (Figure 3a) shows a main resonance at $\delta(^{11}B)$ = 97.2 ppm. This signal corresponds to the resonances of pure MgB_2. This indicates that upon milling no boron-containing phases different from MgB_2 are formed. In the ^{11}B MAS NMR spectrum of the CaH_2 + MgB_2 system after the first hydrogenation cycle (Figure 3b) the signal of α-$Ca(BH_4)_2$ at $\delta(^{11}B)$ = −29.9 ppm dominates the spectrum with an unresolved shoulder at $\delta(^{11}B)$ = −32.7 ppm from β-$Ca(BH_4)_2$ and the presence of a small fraction unreacted MgB_2 as seen by the resonance at $\delta(^{11}B)$ = 97.2 ppm.[7] In addition, a very small resonance at $\delta(^{11}B)$ = 1.3 ppm is observed, which is most likely related to the presence of a tiny amount of tetrahedral BO_4 units. The ^{11}B MAS NMR spectrum of CaH_2 + MgB_2 after the fifth hydrogenation cycle (Figure 3c) reveals the presence of several boron-containing compounds not visible in the PXD analysis presented in Figure 2. In fact, besides the presence of small amounts of α-$Ca(BH_4)_2$ at $\delta(^{11}B)$ = −29.9 ppm and β-$Ca(BH_4)_2$ seen by the shoulder at $\delta(^{11}B)$ = −32.7 ppm, two new phases with center band resonances roughly at $\delta(^{11}B)$ = 5 ppm and −14.4 ppm are observed. These two new signals contain 64% of the total intensity for the center bands and can be assigned to amorphous boron and $CaB_{12}H_{12}$, respectively.[7]

The $3CaH_2$ + CaF_2 + $4MgB_2$ system has also been investigated by MAS NMR. In particular, ^{11}B and ^{19}F MAS NMR spectra were acquired for these samples after the milling procedure (Figures 4b and 5c), after the first hydrogenation cycle (Figures 4c and 5d), and after the fifth hydrogenation cycle (Figures 4d and 5e) to reveal the amorphous/nanocrystalline boron/fluorine-containing phases and their evolution over the hydrogenation cycles. The ^{11}B MAS NMR spectrum of the ball-milled $3CaH_2$ + CaF_2 + $4MgB_2$ sample (Figure 4b) shows two resonances with center bands at $\delta(^{11}B)$ = 97.2 and ∼0 ppm with relative center band intensitities of 87% and 13%, respectively, as observed for the ^{11}B MAS NMR spectrum of the milled CaH_2 + MgB_2 sample. These signals can be attributed to pure MgB_2 and possibly boron oxide impurities (BO_3 and/or BO_4 units). For comparison, the ^{11}B MAS NMR spectrum of pristine MgB_2 is shown in Figure 4a. In the ^{11}B MAS NMR spectrum of $3CaH_2$ + CaF_2 + $4MgB_2$ after the first hydrogenation cycle the signal of α-$Ca(BH_4)_2$ at $\delta(^{11}B)$ =

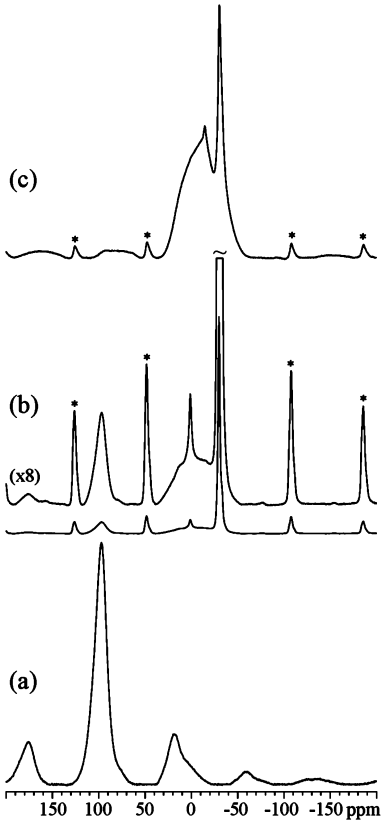

Figure 3. $^{11}B\{^1H\}$ MAS NMR spectra of CaH_2 + MgB_2 after (a) the ball-milling procedure, (b) the first hydrogenation cycle, and (c) the fifth hydrogenation cycle, obtained at 9.4 T using a spinning speed of ν_R = 10.0 kHz. Asterisks in b and c indicate spinning side band from $Ca(BH_4)_2$.

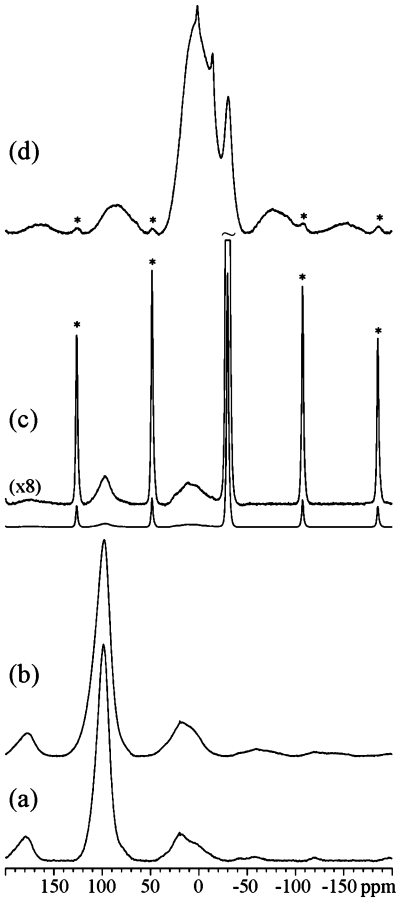

Figure 4. $^{11}B\{^1H\}$ MAS NMR spectra (9.4 T, ν_R = 10.0 kHz) of (a) pristine MgB_2, (b) $3CaH_2$ + CaF_2 + $4MgB_2$ after mechanochemical treatment, (c) after the first hydrogenation cycle, and (d) after the fifth hydrogenation cycle. Asterisks in c and d indicate spinning side band from $Ca(BH_4)_2$. Vertical expansion (×8) of the spectrum in c is shown to illustrate the center band resonances from the minor fractions of MgB_2 and BO_3/BO_4 species.

dx.doi.org/10.1021/jp508780b | J. Phys. Chem. C 2014, 118, 28409−28417

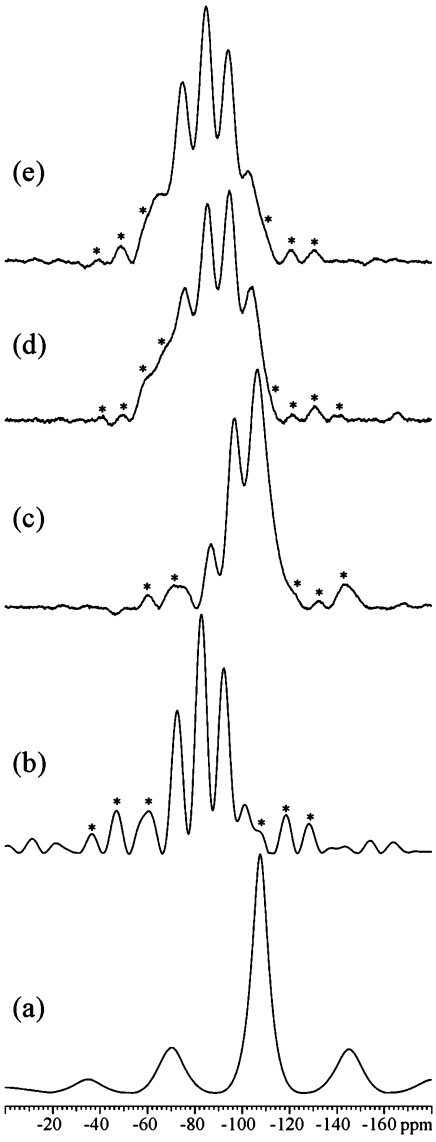

Figure 5. ^{19}F MAS NMR spectra (7.1 T, ν_R = 10.0 kHz) of the samples: (a) pristine CaF_2, (b) solid solution of $CaF_{2-x}H_x$, prepared starting from CaF_2 and CaH_2, and (c) milled $3CaH_2 + CaF_2 + 4MgB_2$, (d) sample after the first hydrogenation cycle, and (e) sample after the fifth hydrogenation cycle. Asterisks in b–e indicate first-order spinning side bands.

−29.6 ppm and a small signal of unreacted MgB_2 at $\delta(^{11}B)$ = 97.3 ppm are observed. Furthermore, small resonances from boron oxide impurities are also detected at about $\delta(^{11}B) \approx 0$ ppm. Evaluation of the center band intensities in Figure 4c reveals that α-$Ca(BH_4)_2$ is the dominating phase (85%) and that MgB_2 (6%) and the BO_3/BO_4 oxide impurities (9%) are only present as minor phases.

The ^{11}B MAS NMR spectrum of $3CaH_2 + CaF_2 + 4MgB_2$ after the fifth absorption cycle shows the presence of four main resonances. The broad signal at $\delta(^{11}B) \approx 10$ ppm can be attributed to amorphous boron, and it constitutes roughly 80% of the total center band intensity. The signal at $\delta(^{11}B) = -30.6$ ppm is related to the presence of a small amount of α-$Ca(BH_4)_2$ (16% of center band intensity), whereas the signals at $\delta(^{11}B) = -1.8$ and −14.0 ppm can be assigned to impurities of BO_4 species and $CaB_{12}H_{12}$, respectively.

For comparison purposes, ^{19}F MAS NMR spectra of pristine CaF_2 and as-prepared CaF_2–CaH_2 solid solution are shown in Figure 5a and 5b, respectively.

The ^{19}F MAS NMR spectrum of the milled $3CaH_2 + CaF_2 + 4MgB_2$ sample (Figure 5c) shows three main signals at $\delta(^{19}F)$ = −86.2, −95.8, and −105.3 ppm, which can be assigned to the resonances from a substituted $CaF_{2-x}H_x$ solid solution. This indicates that formation of the substituted $CaF_{2-x}H_x$ solid solution takes place already during the milling procedure, which is not clearly detected by PXD. The ^{19}F MAS NMR spectrum of $3CaH_2 + CaF_2 + 4MgB_2$ after the first hydrogen absorption cycle (Figure 5d) contains four distinct resonances at $\delta(^{19}F)$ = −75.4, −85.3, −94.6, and −104.3 ppm. Again, these signals can be assigned also to a $CaF_{2-x}H_x$ solid solution. The ^{19}F MAS NMR spectrum of $3CaH_2 + CaF_2 + 4MgB_2$ after the fifth hydrogenation cycle (Figure 5e) contains five distinct resonances at $\delta(^{19}F)$ = −63, −74.8, −84.7, −94.0, and −103.6 ppm. These signals can be attributed to differently substituted $CaF_{2-x}H_x$ phases. The continuous shift of the resonances of $CaF_{2-x}H_x$ toward lower frequency can be explained by the increase of the fluoride content upon cycling. Attempts to quantify the ^{19}F NMR intensities for the individual resonances are complicated by the significant overlap of the different center bands and spinning side bands (marked by asterisks in Figure 5). Thus, improved spectra for these samples could be obtained by applying a somewhat higher spinning speed than ν_R = 10.0 kHz used in this study. However, such a MAS NMR probe, capable of achieving a higher spinning speed and detecting ^{19}F, is currently not available for us.

The effect of the partial replacement of CaH_2 with CaF_2 on the hydrogen sorption properties of the mixed system $CaH_2 + MgB_2$ was also investigated by means of the HP-DSC technique. The first hydrogen absorption reactions of the systems $CaH_2 + MgB_2$ and $3CaH_2 + CaF_2 + 4MgB_2$ were also investigated by HP-DSC. Figure 6 shows the HP-DSC curves recorded for systems $CaH_2 + MgB_2$ (curve a) and $3CaH_2 + CaF_2 + 4MgB_2$ (curve b). Curve a shows upon heating a single exothermic signal with onset at 280 °C and the maximum at roughly 350 °C. During cooling no signal is observed in both curves.

In the curve b, upon heating a first endothermic signal with an onset temperature at 260 °C is observed to precede an exothermic signal with an onset temperature at 280 °C. During cooling, a broad exothermic signal is observed between 230 and 150 °C.

In order to clarify the undergoing absorption reaction mechanisms, in situ SR-PXD analyses were performed for all investigated systems. The temperature and hydrogen pressure applied during the measurements matched the conditions applied earlier in the HP-DSC experiments. Figure 7 shows the measurement carried out for the system $CaH_2 + MgH_2$. The material was heated up to 400 °C with a constant heating rate of 5 °C/min and then kept for several hours at 400 °C. The applied hydrogen pressure was 130 bar H_2. These conditions apply to all performed in situ SR-PXD analyses. The phases in the starting material are CaH_2 and MgB_2 as well as a small amount of CaO. Upon heating, due to thermal expansion, all peaks shift toward lower q values. At approximately 370 °C, formation of β-$Ca(BH_4)_2$ takes place simultaneously with formation of $Ca_4Mg_3H_{14}$. The isothermal period at 400 °C is characterized by the intensity increment of the diffracted peaks of β-$Ca(BH_4)_2$ and $Ca_4Mg_3H_{14}$ and the intensity decrement of the starting reactants diffraction peaks. Among the final

dx.doi.org/10.1021/jp508780b | J. Phys. Chem. C 2014, 118, 28409–28417

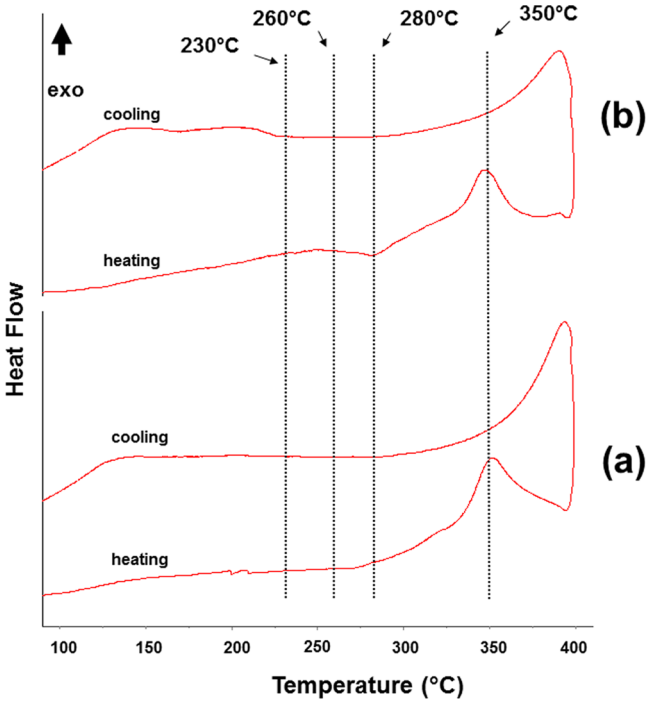

Figure 6. HP-DSC curves of CaH_2 + MgB_2 (a) and $3CaH_2$ + CaF_2 + $4MgB_2$ (b) hydrogen absorption reactions measured at 130 bar of hydrogen pressure from RT to 400 °C and subsequently cooled using a heating/cooling rate of 5 °C/min.

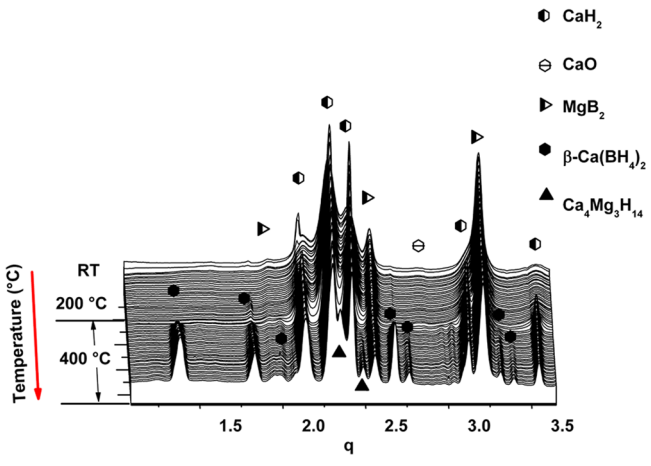

Figure 7. Series of SR-PXD patterns of the CaH_2 + MgH_2 system heated under 130 bar of hydrogen pressure from RT to 400 °C using a heating rate of 5 °C/min.

products β-$Ca(BH_4)_2$ and $Ca_4Mg_3H_{14}$, also residual MgB_2 and CaH_2 are observed.

In situ SR-PXD analysis of the absorption reaction for the system $3CaH_2$ + CaF_2 + $4MgB_2$ is reported in Figure 8. The starting material consists of CaH_2, MgB_2, CaO, and, as seen in the MAS NMR analysis of Figure 5, $CaF_{2-x}H_x$. The heating period is characterized by a fast intensity increase of the diffracted peaks of the $CaF_{2-x}H_x$ phase between 220 and 330 °C and simultaneous decrement of the CaH_2 peaks. This effect is due to further formation of the $CaF_{2-x}H_x$ solid solution, indicated also by the appearance of the peak (200) at q = 2.3 $Å^{-1}$. The remaining heating time and isothermal period at 400 °C are characterized by formation of β-$Ca(BH_4)_2$ (started at 390 °C) and its growth. It must be noticed that in the observed

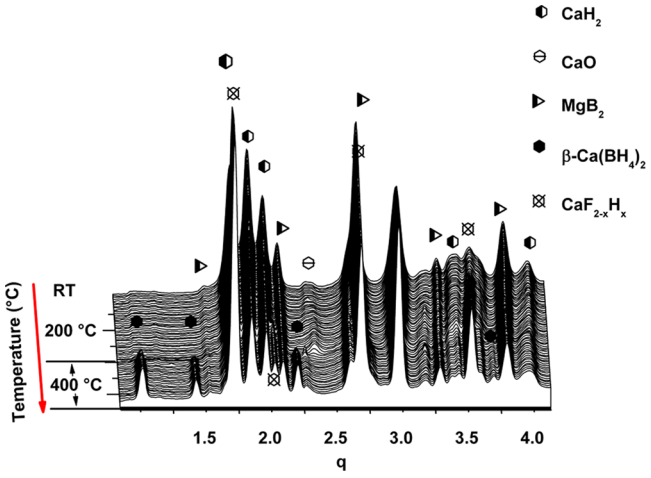

Figure 8. Series of SR-PXD patterns of the $3CaH_2$ + CaF_2 + $4MgB_2$ system heated under 130 bar of hydrogen pressure from RT to 400 °C using a heating rate of 5 °C/min.

period of time formation of $Ca_4Mg_3H_{14}$ or Mg-containing phases was not detected. This might be due to a possible overlapping with the peaks of the other phases.

In order to investigate the effect of the $CaF_{2-x}H_x$ solid solution formation on the hydrogen absorption properties of the system $3CaH_2$ + CaF_2 + $4MgB_2$, a sample containing $CaF_{2-x}H_x$ (prepared starting from a mixture of CaH_2 and CaF_2 in a molar ratio 1:1) and MgB_2 was prepared and investigated using the in situ SR-PXD technique (Figure 9). The first SR-

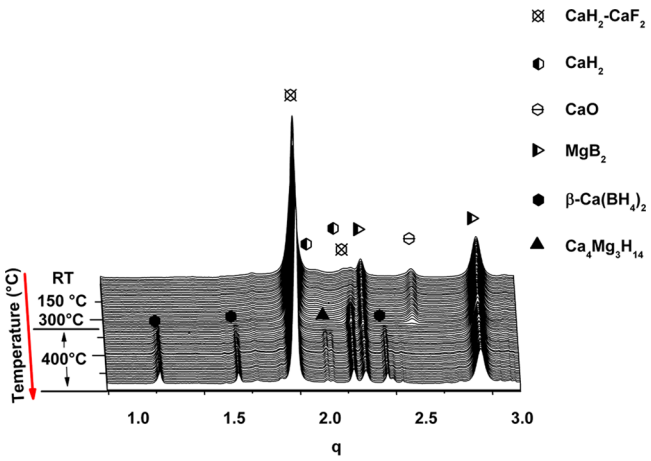

Figure 9. Series of SR-PXD patterns of the CaF_2–CaH_2 + MgB_2 system heated under 130 bar of hydrogen pressure from RT to 400 °C using a heating rate of 5 °C/min.

PXD pattern recorded at RT shows the diffracted reflections of CaH_2–CaF_2 ($CaF_{2-x}H_x$), MgB_2, and small amounts of CaH_2 and CaO. Upon heating, no changes are observed in the system. During the isothermal period at 400 °C, formation of small amounts of β-$Ca(BH_4)_2$ and $Ca_4Mg_3H_{14}$ is visible. Formation of β-$Ca(BH_4)_2$ and $Ca_4Mg_3H_{14}$ stops immediately after CaH_2 is consumed. Interestingly, together with formation of $Ca(BH_4)_2$ and $Ca_4Mg_3H_{14}$, the reflections of CaO disappear. Although the reason behind the disappearance of CaO is not yet clear, formation of an amorphous hydride phase containing calcium and oxygen and/or nanosized MgO might be a possible explanation.[39]

dx.doi.org/10.1021/jp508780b | J. Phys. Chem. C 2014, 118, 28409–28417

DISCUSSION

Assuming that the systems $CaH_2 + MgB_2$ and $3CaH_2 + CaF_2 + 4MgB_2$ follow the reaction paths proposed in reaction 9 or 10, they are expected to show reversible gravimetric hydrogen capacities of 8.4 and 7.7 wt %, respectively.

$$CaH_2 + MgB_2 + 4H_2 \leftrightarrow Ca(BH_4)_2 + MgH_2 \quad (9)$$

$$3CaH_2 + CaF_2 + 4MgB_2 + 12H_2 \leftrightarrow 4Ca(BH_4)_2 + 3MgH_2 + MgF_2 \quad (10)$$

The results of the volumetric measurements, however, reveal gravimetric hydrogen capacities far below the theoretical values for both $CaH_2 + MgB_2$ and $3CaH_2 + CaF_2 + 4MgB_2$. Moreover, the hydrogen content of both systems drastically decreases upon cycling (Figure 1). In the first dehydrogenation reaction the $CaH_2 + MgB_2$ system desorbs an amount of hydrogen equal to ~74% of the theoretical hydrogen capacity. Sieverts measurements reveal further decay of the dehydrogenation capacity of the second, third, and fourth cycles to 70%, 50%, and 43%, respectively. The corresponding values for the $3CaH_2 + CaF_2 + 4MgB_2$ system are approximately 56%, 51%, 43%, and 43%. The first dehydrogenation capacity of both systems differs significantly with respect to their theoretical capacities and with respect to each other. This behavior indicates dissimilar reaction mechanisms between these two systems. Indeed, in situ SR-PXD measurement of the hydrogenation process of $CaH_2 + MgB_2$ shows a single-step reaction mechanism (Figure 7). The appearance of the diffracted peaks of β-$Ca(BH_4)_2$ and $Ca_4Mg_3H_{13}$ occurs simultaneously at 350 °C; then the intensity of these reflections increases during the remaining heating period and isothermal treatment at 400 °C. On the basis of these results, the absorption reaction mechanism for $CaH_2 + MgB_2$ can be explained as follows: first CaH_2, MgB_2, and H_2 react to form β-$Ca(BH_4)_2$, and then Mg reacts with the remaining CaH_2 and H_2 to produce $Ca_3Mg_4H_{14}$. Following this reaction mechanism an imbalance of molar ratio between CaH_2 and MgB_2 is created. As a consequence, an excess of unreacted MgB_2 remains as a final product. Indeed, in the ^{11}B MAS NMR spectrum of the first hydrogenated $CaH_2 + MgB_2$ the signal of MgB_2 is present (Figure 3b). This explains why the theoretical capacity (which assumes 1:1 molar ratio between CaH_2 and MgB_2) is not achieved. To understand better the degradation of the hydrogen capacity of the system over the hydrogenation cycles, the amorphous boron-containing compounds formed upon cycling must be taken into account. It is known from the literature that $Ca(BH_4)_2$ decomposes to CaH_2, CaB_6, $CaB_{12}H_{12}$, and amorphous boron. The amorphous boron and $CaB_{12}H_{12}$ are highly stable products, and their formation reduces the amount of reactive boron, which can form $Ca(BH_4)_2$. MgB_2, which does not react during the first absorption process, is consumed to form $Ca(BH_4)_2$ during the second hydrogenation process. Consequently, the capacity value of the second dehydrogenation is still close to the first one. However, over the hydrogenation cycles the hydrogen capacity is further lowered. The ^{11}B MAS NMR spectrum of the sample after the fifth absorption shows formation of significant amounts of $CaB_{12}H_{12}$ and amorphous boron (Figure 3c), corresponding to 67% of the total center band intensity. Since the system is impoverished of reactive boron compounds (e.g., CaB_6), formation of $Ca(BH_4)_2$ is suppressed. As a consequence, the reversible hydrogen storage capacity of the system shifts toward the only reversible compound, namely, $Ca_3Mg_4H_{14}$. This explains the continuous reduction of hydrogen content of the $CaH_2 + MgB_2$ composite system upon cycling, leading to a constant capacity value. In fact, ex situ PXD measurements of the hydrogenated samples after the first, third, and fifth hydrogenation cycles show a clear increase of the diffracted peak intensities of the ternary hydride $Ca_3Mg_4H_{14}$ and a simultaneous decrement of those of $Ca(BH_4)_2$ (Figure 2).

In the case of the $3CaH_2 + CaF_2 + 4MgB_2$ system, however, the in situ SR-PXD measurement shows a two-step reaction mechanism (Figure 4). In the first step, between 220 and 330 °C, the intensities of the diffracted peaks of CaH_2 decrease, whereas the intensities of the $CaF_{2-x}H_x$ solid solution peaks increase. Then, in a second step at about 390 °C, the diffraction peaks of β-$Ca(BH_4)_2$ phase appear.

Although with slightly different temperature onset for the first event, these two steps are also visible in the HP-DSC curve b of Figure 6. The broad exothermic peak observed for the same curve during cooling can be related to partial disproportionation of CaH_2 from the formed $CaF_{2-x}H_x$ solid solution.

The degradation mechanism observed here deviates from previous investigations of the $NaBH_4$−$NaBF_4$ system. Here the fluorine-containing compound is less stable as compared to the reaction product NaF; furthermore, there is a tendency for this system to form gaseous decomposition products, B_2H_6 and BF_3, which lead to formation of significant amounts of $Na_2B_{12}H_{12}$.[40] A more stable fluorine-containing compound was selected for the present investigation but turns out to form stable solid solutions, which also hamper the hydrogen storage properties.

Though the hydrogenation reaction (the second step) of $3CaH_2 + CaF_2 + 4MgB_2$ is equivalent to that of $CaH_2 + MgB_2$, the amount of hydrogen released during the first desorption process (56% with respect to the theoretical value) is significantly lower than the corresponding value (74%) for the unfluorinated system ($CaH_2 + MgB_2$). This phenomenon can be explained by examining the first reaction step in detail. Here, chemical interaction of CaH_2 and CaF_2 leads to formation of more stable solid solution $CaF_{2-x}H_x$, which reduces the amount of CaH_2 available in the system to form $Ca(BH_4)_2$ (Figure 9). In addition, already during the ball milling of the starting reactants a fraction of CaH_2 and CaF_2 is converted into $CaF_{2-x}H_x$ (Figure 5a), which reduces the amount of free CaH_2 even further. A comparison between the ^{19}F MAS NMR spectra of as-milled, the first and fifth absorbed samples reveal that the amount of solid solution $CaF_{2-x}H_x$ present in the system increases with the hydrogenation cycles. Thus, the residual CaH_2 reacts with MgB_2 to form $Ca(BH_4)_2$, following a reaction mechanism which traces out the one of the pristine $CaH_2 + MgB_2$ system. This is clearly visible in the PXD analyses (Figure 2) and in the ^{11}B MAS NMR spectra (Figure 4). Therefore, the faster reduction of the hydrogen capacity observed for the system $3CaH_2 + CaF_2 + 4MgB_2$ in comparison to the system $CaH_2 + MgB_2$ is a consequence of $CaF_{2-x}H_x$ formation, which reduces the amount of CaH_2 available to form first $Ca(BH_4)_2$ and then $Ca_3Mg_4H_{14}$.

CONCLUSION

The effect of a partial replacement of CaH_2 by CaF_2 on the sorption properties of the system $CaH_2 + MgB_2$ was studied. It was found that addition of CaF_2 to $CaH_2 + MgB_2$ has a detrimental effect on the system reversibility. In fact, replacement of CaH_2 with CaF_2 leads to a faster decrement

of the hydrogen capacity of the system upon cycling. The explanation of the observed phenomenon is formation of the solid solution $CaF_{2-x}H_x$, which reduces the amount of CaH_2 available to form first $Ca(BH_4)_2$ and then $Ca_3Mg_4H_{14}$. The amount of solid solution $CaF_{2-x}H_x$, which forms already during the milling process, increases upon cycling. $CaF_{2-x}H_x$ appears to be more stable than CaH_2 and does not react with MgB_2 and presumably also not with CaB_6 to form $Ca(BH_4)_2$.

AUTHOR INFORMATION

Corresponding Author

*E-mail: claudio.pistidda@hzg.de.

Present Address

◊Institute of Nanotechnology, Karlsruhe Institute of Technology, Hermann-von-Helmholtz-Platz 17, 6344 Eggenstein-Leopoldshafen, Germany.

Notes

The authors declare no competing financial interest.

ACKNOWLEDGMENTS

This work was supported by the Danish National Research Foundation, Center for Materials Crystallography (DNRF93), the Danish Strategic Research Council (the research project HyFillFast), and the Danish Research Council for Nature and Universe (Danscatt). We are grateful to the Carlsberg Foundation. Access to beamtime at the MAX-II synchrotron, Lund, Sweden in the research laboratory MAX-lab is gratefully acknowledged. We also acknowledge funding from the European Community's Seventh Framework Programme, The Fuel Cells and Hydrogen Joint Undertaking (FCH JU), project BOR4STORE (303428), the Marie Curie Initial Network ECOSTORE under grant agreement (607040) and the COST Action MP1103 "Nanostructured materials for solid-state hydrogen storage". We express our sincere gratitude to Ms. Lucia Anna Pistidda, Ms. Adele Garroni, and Ms. Emma Luisa Bonatto Minella for their support.

REFERENCES

(1) Grochala, W.; Edwards, P. P. Thermal Decomposition of the Non-Interstitial Hydrides for the Storage and Production of Hydrogen. *Chem. Rev.* **2004**, *104*, 1283−1315.

(2) Vajo, J. J.; Olson, G. L. Hydrogen Storage in Destabilized Chemical Systems. *Scr. Mater.* **2007**, *56*, 829−834.

(3) Züttel, A.; Rentsch, S.; Fischer, P.; Wenger, P.; Sudan, P.; Mauron, P.; Emmenegger, C. Hydrogen Storage Properties of $LiBH_4$. *J. Alloys Compd.* **2003**, *356*−*357*, 515−520.

(4) Kim, J. H.; Jin, S. A.; Shim, J. H.; Cho, Y. W. Reversible Hydrogen Storage in Calcium Borohydride $Ca(BH_4)_2$. *Scr. Mater.* **2008**, *58*, 481−483.

(5) Barkhordarian, G.; Jensen, T. R.; Doppiu, S.; Bösenberg, U.; Borgschulte, A.; Gremaud, R.; Cerenius, Y.; Dornheim, M.; Klassen, T.; Bormann, R. Formation of Ca(BH4)2 from Hydrogenation of CaH_2 + MgB_2 Composite. *J. Phys. Chem. C* **2008**, *112*, 2743−2749.

(6) Barkhordarian, G.; Klassen, T.; Dornheim, M.; Bormann, R. Unexpected Kinetic Effect of MgB_2 in Reactive Hydride Composites Containing Complex Borohydrides. *J. Alloys Compd.* **2007**, *440*, L18−L21.

(7) Bonatto Minella, C.; Garroni, S.; Olid, D.; Teixidor, F.; Pistidda, C.; Lindemann, I.; Gutfleisch, O.; Baró, M. D.; Bormann, R.; Klassen, T.; et al. Experimental Evidence of $Ca[B_{12}H_{12}]$ Formation During Decomposition of a $Ca(BH_4)_2$ + MgH_2 Based Reactive Hydride Composite. *J. Phys. Chem. C* **2011**, *115*, 18010−18014.

(8) Bösenberg, U.; Doppiu, S.; Mosegaard, L.; Barkhordarian, G.; Eigen, N.; Borgschulte, A.; Jensen, T. R.; Cerenius, Y.; Gutfleisch, O.; Klassen, T.; et al. Hydrogen Sorption Properties of MgH_2-$LiBH_4$ Composites. *Acta Mater.* **2007**, *55*, 3951−3958.

(9) Bösenberg, U.; Kim, J. W.; Gosslar, D.; Eigen, N.; Jensen, T. R.; Bellosta von Colbe, J. M.; Zhou, Y.; Dahms, M.; Kim, D. H.; Gunther, R.; et al. Role of Additives in $LiBH_4$-MgH_2 Reactive Hydride Composites for Sorption Kinetics. *Acta Mater.* **2010**, *58*, 3381−3389.

(10) Deprez, E.; Muñoz-Márquez, M. A.; Jimenez de Haro, M. C.; Palomares, F. J.; Soria, F.; Dornheim, M.; Bormann, R.; Fernández, A. Combined X-ray Photoelectron Spectroscopy and Scanning Electron Microscopy Studies of the $LiBH_4$-MgH_2 Reactive Hydride Composite With and Without a Ti-based Additive. *J. Appl. Phys.* **2011**, *109*, 014913.

(11) Garroni, S.; Milanese, C.; Girella, A.; Marini, A.; Mulas, G.; Menendez, E.; Pistidda, C.; Dornheim, M.; Surinach, S.; Baró, M. D. Sorption Properties of $NaBH_4/MH_2$ (M = Mg, Ti) Powder Systems. *Int. J. Hydrogen Energy* **2010**, *35*, 5434−5441.

(12) Garroni, S.; Milanese, C.; Pottmaier, D.; Mulas, G.; Nolis, P.; Girella, A.; Caputo, R.; Olid, D.; Teixdor, F.; Baricco, M.; et al. Experimental Evidence of $Na_2[B_{12}H_{12}]$ and Na Formation in the Desorption Pathway of the $2NaBH_4$ + MgH_2 System. *J. Phys. Chem. C* **2011**, *115*, 16664−16671.

(13) Garroni, S.; Minella, C. B.; Pottmaier, D.; Pistidda, C.; Milanese, C.; Marini, A.; Enzo, S.; Mulas, G.; Dornheim, M.; Baricco, M.; et al. Mechanochemical Synthesis of $NaBH_4$ Starting from NaH-MgB_2 Reactive Hydride Composite System. *Int. J. Hydrogen Energy* **2013**, *38*, 2363−2369.

(14) Garroni, S.; Pistidda, C.; Brunelli, M.; Vaughan, G. B. M.; Surinach, S.; Baro, M. D. Hydrogen Desorption Mechanism of $2NaBH_4$ + MgH_2 Composite Prepared by High-Energy Ball Milling. *Scr. Mater.* **2009**, *60*, 1129−1132.

(15) Gregory, D. H. Lithium Nitrides, Imides and Amides as Lightweight, Reversible Hydrogen Stores. *J. Mater. Chem.* **2008**, *18*, 2321−2330.

(16) Minella, C. B.; Pistidda, C.; Garroni, S.; Nolis, P.; Baró, M. D.; Gutfleisch, O.; Klassen, T.; Bormann, R. .; Dornheim, M. $Ca(BH_4)_2$ + MgH_2: Desorption Reaction and Role of Mg on Its Reversibility. *J. Phys. Chem. C* **2013**, *117*, 3846−3852.

(17) Pistidda, C.; Barkhordarian, G.; Rzeszutek, A.; Garroni, S.; Minella, C. B.; Baró, M. D.; Nolis, P.; Börmann, R.; Klassen, T.; Dornheim, M. Activation of the Reactive Hydride Composite $2NaBH_4$ + MgH_2. *Scr. Mater.* **2011**, *64*, 1035−1038.

(18) Pistidda, C.; Garroni, S.; Minella, C. B.; Dolci, F.; Jensen, T. R.; Nolis, P.; Bösenberg, U.; Cerenius, Y.; Lohstroh, W.; Fichtner, M.; et al. Pressure Effect on the 2NaH + MgB_2 Hydrogen Absorption Reaction. *J. Phys. Chem. C* **2010**, *114*, 21816−21823.

(19) Pistidda, C.; Napolitano, E.; Pottmaier, D.; Dornheim, M.; Klassen, T.; Baricco, M.; Enzo, S. Structural Study of a New B-rich Phase Obtained by Partial Hydrogenation of 2NaH + MgB_2. *Int. J. Hydrogen Energy* **2013**, *38*, 10479−10484.

(20) Pistidda, C.; Pottmaier, D.; Karimi, F.; Garroni, S.; Rzeszutek, A.; Tolkiehn, M.; Fichtner, M.; Lohstroh, W.; Baricco, M.; Klassen, T.; et al. Effect of NaH/MgB_2 Ratio on the Hydrogen Absorption Kinetics of the System NaH + MgB_2. *Int. J. Hydrogen Energy* **2014**, *39*, 5030−5036.

(21) Vajo, J. J.; Mertens, F.; Ahn, C. C.; Bowman, R. C.; Fultz, B. Altering Hydrogen Storage Properties by Hydride Destabilization through Alloy Formation: LiH and MgH_2 Destabilized with Si. *J. Phys. Chem. B* **2004**, *108*, 13977−13983.

(22) Bonatto Minella, C.; Garroni, S.; Pistidda, C.; Gosalawit-Utke, R.; Barkhordarian, G.; Rongeat, C.; Lindemann, I.; Gutfleisch, O.; Jensen, T. R.; Cerenius, Y.; et al. Effect of Transition Metal Fluorides on the Sorption Properties and Reversible Formation of $Ca(BH_4)_2$. *J. Phys. Chem. C* **2011**, *115*, 2497−2504.

(23) Bonatto Minella, C.; Pellicer, E.; Rossinyol, E.; Karimi, F.; Pistidda, C.; Garroni, S.; Milanese, C.; Nolis, P.; Baró, M. D.; Gutfleisch, O.; et al. Chemical State, Distribution, and Role of Ti- and Nb-Based Additives on the $Ca(BH_4)_2$ System. *J. Phys. Chem. C* **2013**, *117*, 4394−4403.

(24) Jepsen, L. H.; Ley, M. B.; Lee, Y. S.; Cho, Y. W.; Dornheim, M.; Jensen, J. O.; Filinchuk, Y.; Jørgensen, J. E.; Besenbacher, F.; Jensen, T. R. Boron-Nitrogen Based Hydrides and Reactive Composites for Hydrogen Storage. *Mater. Today* **2014**, *17*, 129−135.
(25) Ley, M. B.; Jepsen, L. H.; Lee, Y. S.; Cho, Y. W.; Bellosta von Colbe, J. M.; Dornheim, M.; Rokni, M.; Jensen, J. O.; Sloth, M.; Filinchuk, Y.; et al. Complex Hydrides for Hydrogen Storage-New Perspectives. *Mater. Today.* **2014**, *17*, 122−128.
(26) Kim, Y.; Reed, D.; Lee, Y. S.; Lee, J. Y.; Shim, J. H.; Book, D.; Cho, Y. W. Identification of the Dehydrogenated Product of $Ca(BH_4)_2$. *J. Phys. Chem. C* **2009**, *113*, 5865−5871.
(27) Ozoliņš, V.; Majzoub, E. H.; Wolverton, C. First-Principles Prediction of Thermodynamically Reversible Hydrogen Storage Reactions in the Li-Mg-Ca-B-H System. *J. Am. Chem. Soc.* **2008**, *131*, 230−237.
(28) Zhang, Y.; Majzoub, E.; Ozoliņš, V.; Wolverton, C. Theoretical Prediction of Different Decomposition Paths for $Ca(BH_4)_2$ and $Mg(BH_4)_2$. *Phys. Rev. B* **2010**, *82* (17), 174107.
(29) Kim, Y.; Hwang, S. J.; Lee, Y. S.; Suh, J. Y.; Han, H. N.; Cho, Y. W. Hydrogen Back-Pressure Effects on the Dehydrogenation Reactions of $Ca(BH_4)_2$. *J. Phys. Chem. C* **2012**, *116*, 25715−25720.
(30) Kim, Y.; Hwang, S. J.; Shim, J. H.; Lee, Y. S.; Han, H. N.; Cho, Y. W. Investigation of the Dehydrogenation Reaction Pathway of $Ca(BH_4)_2$ and Reversibility of Intermediate Phases. *J. Phys. Chem. C* **2012**, *116*, 4330−4334.
(31) Kim, J. H.; Shim, J. H.; Cho, Y. W. On the Reversibility of Hydrogen Storage in Ti- and Nb-catalyzed $Ca(BH_4)_2$. *J. Power Sources* **2008**, *181*, 140−143.
(32) Rönnebro, E.; Majzoub, E. H. Calcium Borohydride for Hydrogen Storage: Catalysis and Reversibility. *J. Phys. Chem. B* **2007**, *111*, 12045−12047.
(33) Brinks, H. W.; Fossdal, A.; Hauback, B. C. Adjustment of the Stability of Complex Hydrides by Anion Substitution. *J. Phys. Chem. C* **2008**, *112*, 5658−5661.
(34) Eigen, N.; Bösenberg, U.; Bellosta von Colbe, J. M.; Jensen, T. R.; Cerenius, Y.; Dornheim, M.; Klassen, T.; Bormann, R. Reversible Hydrogen Storage in NaF-Al Composites. *J. Alloys Compd.* **2009**, *477*, 76−80.
(35) Clausen, B. S.; Steffensen, G.; Fabius, B.; Villadsen, J.; Feidenhansl, R.; Topsoe, H. In Situ Cell for Combined XRD and Online Catalysis Tests - Studies of Cu-based Water Gas Shift and Methanol Catalysts. *J. Catal.* **1991**, *132*, 524−535.
(36) Rodriguez, J. A.; Hanson, J. C.; Frenkel, A. I.; Kim, J. Y.; Perez, M. Experimental and Theoretical Studies on the Reaction of H-2 with NiO: Role of O Vacancies and Mechanism for Oxide Reduction. *J. Am. Chem. Soc.* **2002**, *124*, 346−354.
(37) Bösenberg, U.; Doppiu, S.; Mosegaard, L.; Barkhordarian, G.; Eigen, N.; Borgschulte, A.; Jensen, T. R.; Cerenius, Y.; Gutfleisch, O.; Klassen, T.; et al. Hydrogen Sorption Properties of MgH_2-$LiBH_4$ Composites. *Acta Mater.* **2007**, *55*, 3951−3958.
(38) http://www.esrf.eu/computing/scientific/FIT2D/.
(39) Riktor, M. D.; Filinchuk, Y.; Vajeeston, P.; Bardaji, E. G.; Fichtner, M.; Fjellvag, H.; Sorby, M. H.; Hauback, B. C. The Crystal Structure of the First Borohydride Borate, $Ca_3(BD_4)_3(BO_3)$. *J. Mater. Chem.* **2011**, *21*, 7188−7193.
(40) Rude, L. H.; Filso, U.; D'Anna, V.; Spyratou, A.; Richter, B.; Hino, S.; Zavorotynska, O.; Baricco, M.; Sorby, M. H.; Hauback, B. C.; et al. Hydrogen-Fluorine Exchange in $NaBH_4$-$NaBF_4$. *Phys. Chem. Chem. Phys.* **2013**, *15*, 18185−18194.